# Evolution of ITZ and its effect on the carbonation depth of concrete under supercritical $CO_2$ condition

Hao Bao [a,b,*], Gang Xu [a,b], Min Yu [c,*], Qing Wang [a,b], Rende Li [b], Mohamed Saafi [d], Jianqiao Ye [d,*]

a. Hubei Key Laboratory of Disaster Prevention and Mitigation, China Three Gorges University, Yichang, China

b. College of Civil Engineering & Architecture, China Three Gorges University, Yichang, China

c. School of Civil Engineering, Wuhan University, Wuhan, China

d. Department of Engineering, Lancaster University, Lancaster LA1 4YR, UK

* Correspondence author: baohaowhu@163.com (H. Bao), ceyumin@whu.edu.cn (M. Yu), j.ye2@lancaster.ac.uk (J. Ye)

**Abstract:** In this paper, supercritical carbonation tests of concrete specimens with different water-to-cement ratios are carried out. In the test, the thickness of interfacial transition zone (ITZ) of the concrete is determined by the distribution of Ca/Si ratio across the interface between the coarse aggregate and cement paste. The microhardness distribution, microstructure and porosity of the ITZ before and after supercritical carbonation are analyzed. A geometrical and physical model considering the distribution of porosity, coarse aggregates, ITZ, and the supercritical carbonation of concrete is proposed, by which cracks, pores, calcium carbonates, and C-S-H gel at the interface of coarse aggregates and cement paste can be studied. The overall microstructures are relatively compacted after supercritical carbonation. The thickness of ITZ of concrete is reduced from 47-79 μm to 35-51 μm after supercritical carbonation. The average value and variance of carbonation depth of concrete increase with the increase of the thickness and porosity of ITZ. Comparing the carbonation results of concrete with different thicknesses and porosity of ITZ, it appears that porosity of ITZ has greater impact on the carbonation depth of concrete.

**Keywords:** Concrete; Interfacial transition zone; Supercritical carbonation; Geometrical and physical model; Carbonation depth.

## 1. Introduction

Properties of concrete, such as permeability [1,2] and corrosion resistance [3,4], have been studied extensively by both engineers and researchers. It is well known now that concrete durability is greatly influenced by the internal structural characteristics of the materials [5], among which ITZ has higher porosity [6] and lower hardness [7], and contains more calcium hydroxide with lower compactness [8]. Thus, an ITZ has weaker mechanical properties than cement slurry [9], which presents a weak link of the internal structure of concrete materials [10-14]. The influence of ITZ between cement paste and aggregates on the carbonation of concrete has been studied recently [15,16]. It is not unusual that initial cracks of concrete may occur near ITZ [17] due to inhomogeneity, and the ITZ around aggregates may network with each other, resulting in enhanced $CO_2$ diffusion [18]. Clearly, an ITZ is an important channel for $CO_2$ transmission in concrete. The transport of $CO_2$ in concrete and the carbonation reaction will inevitably damage the passivation film on the surface of steel bars in concrete structures, cause corrosion of reinforcements [19], and finally lead to failure and a reduction in service life of structures [20]. Therefore, studies on microscopic characteristics of ITZ and the effect of ITZ on the carbonation process of concrete will provide a further understanding of the role of ITZ in carbonation and the effect of ITZ on the durability design of reinforced concrete structures.

The origin of ITZ lies in the packing of anhydrous cement grains from less than a micron to up to 100 μm against aggregate particles with a magnitude several order larger [21]. Current research on microscopic characteristics of an ITZ mainly focuses on its thickness, micro-hardness, porosity, and pore distribution [22-24]. The thickness of an ITZ is mainly affected by the water-binder ratio [25-27], size and type of aggregate [28,29], and generally defined by ITZ hardness, porosity, unhydrated cement, and other indicators compared with cement paste [30,31]. Multiple factors lead to the formation of an ITZ, including wall effect [32], one-side growth [33], water films, filtration effects of cement grains, micro-bleeding, and gel syneresis [33]. The wall effect is about the packing of the anhydrous cement grains against the relative flat aggregate surface [36]. Due to a wall effect that causes inefficient packing of the cement particles near the aggregates, the ITZ regions will initially have a higher water-binder ratio and a larger interparticle spacing than the bulk cement paste [37]. A lower water-binder ratio of concrete will generally lead to denser and more uniform cement paste and thinner ITZ [38]. ITZ thickness was experimentally evaluated in the range of 10 μm~100 μm [27,28]. The micro-hardness of ITZ of cement-based materials can be tested by nanoindentation [39]. The hardness of an ITZ is correlated with the porosity of the ITZ [31], which is one of the important ITZ microscopic characteristics. The hardness and elastic modulus of ITZ are lower than those of cement paste. In addition, the hardness of an ITZ can be affected by water-cement ratios, aggregate type, size of aggregates, and curing age [40]. The compactness of an ITZ can be improved by the addition of fly ash in concrete, and hydrated and unhydrated products can be distinguished by their microhardness [40]. The porosity and pore distribution of an ITZ are important indexes to characterize the performance of the ITZ. The porosity of concrete ITZ is greater than that of cement paste [41,42], which can be affected by the water-cement ratio, aggregate size and type, content of initial unhydrated cement particles during the casting of concrete, and the compactness of the concrete. When the water-cement ratios are the same, the porosity of ITZ decreases with the decrease of aggregate size and increase of curing age [43]. The transition zone can be densified by, e.g., adding silica fume in concrete. The strength of high-strength silica fume concretes is usually attributed to the reduction in w/c ratio and the refinement of the pore structure [44].

The effects of ITZ on the carbonation performance of concrete were investigated based on accelerated laboratory carbonation tests [18,45]. The ITZ of concrete becomes more compact and the compressive strength was improved after the carbonation treatment [46]. The distribution of the carbonation zone was changed by the evolution of ITZ [47]. However, it took 7 days to obtain a carbonation depth of 9 mm by the accelerated laboratory carbonation test with the relative humidity and temperature of 55% and 26℃, respectively [48]. The supercritical carbonation technology, as an efficient method of carbonation treatment of concrete, can greatly shorten the carbonation time, and it took only 7.5 hours to reach a carbonation depth of 10 mm [49]. Supercritical carbonation techniques have become a promising and time-saving method in the material surface curing, improving compactness of materials [50-52], enhancing mechanical property and durability of fiber reinforced cementitious composites, recycling concrete [53], and solidification and stabilization of heavy metals and hazardous materials [54-56] in concrete. Carbonation depth is a significant parameter to evaluate the degree of supercritical carbonation treatment of concrete [57]. $CO_2$ is in the supercritical state when the temperature of $CO_2$ exceeds 31.1℃ and the pressure exceeds 7.38 MPa [49]. The viscosity and diffusion coefficients of supercritical $CO_2$ are close to that of gas, and its density is close to that of liquid, which makes it possible for the $CO_2$ to quickly penetrate into the concrete [58] and accelerate the carbonation of concrete. Furthermore, the percolation and transport properties of concrete will be affected by the existence of ITZ [59-61]. However, it is found that the investigations using the supercritical carbonation technology were mainly on cement mortar, while research on the microstructure evolution of ITZ of concrete is rare. As mentioned above, ITZ is an important channel for $CO_2$ transmission in concrete, which will inevitably affect carbonation reaction. Consequently, this will affect the carbonation depth of concrete, which is an important index for macroscopic evaluation of the carbonation degree of concrete [62-64]. Thus, to predict and evaluate carbonation depth of concrete under supercritical $CO_2$ condition more accurately, it is necessary to study the influence of ITZ on the supercritical carbonation depth of concrete.

Given the complexity of microstructure evolution of ITZ of concrete under supercritical $CO_2$ condition and its influence on the supercritical carbonation depth of concrete, supercritical carbonation tests on concrete specimens with different water-cement ratios will be carried out in this study. In general, the content of silicon dioxide increases, the content of calcium oxide decreased, and the ratio of calcium to silicon (Ca/Si ratio) increased from aggregate to cement paste [31,65]. The thickness of ITZ can be determined more accurately by the change of Ca/Si ratio. The micro-morphology, calcium-silicon ratio distribution, and hardness distribution around the ITZs before and after supercritical carbonation will be investigated by using the scanning electron microscope test (SEM), and nanoindentation test. The porosity changes of cement paste will be measured by the mercury intrusion porosimetry test. The porosity of an ITZ will be estimated by the relational model between the hardness and porosity of cement paste and ITZ. Furthermore, a geometric and physical model considering the distribution of porosity, coarse aggregates, ITZ, and the supercritical carbonation of concrete is proposed, and the influence of the thickness and porosity of ITZ on the supercritical carbonation depth of concrete will be discussed in this paper.

## 2. Materials and test program

*2.1. Raw materials*

River sands with a fineness modulus of 2.5 were used as the fine aggregates. P.O 42.5 R common Portland cement as supplementary cementing materials were also used in this study. The chemical composition and properties of the commonly used Portland cement were obtained by XRF analysis and are listed in Table 1.

**Table 1** Chemical composition and properties of the cement.

| Components | Contents |
|---|---|
| $SiO_2$ (%) | 21.53 |
| $Al_2O_3$ (%) | 5.07 |
| CaO (%) | 65.69 |
| $Fe_2O_3$ (%) | 2.31 |
| MgO (%) | 1.14 |
| $K_2O$ (%) | 0.36 |
| $Na_2O$ (%) | 0.07 |
| $SO_3$ (%) | 2.5 |
| Loss on ignition (%) | 0.4 |
| Blaine fineness ($m^2$/kg) | 346 |
| Specific gravity (g/$cm^3$) | 3.17 |
| Specific surface area ($cm^2$/g) | 350 |

*2.2. Preparation of concrete specimens*

ITZ in concrete is related to the properties of aggregate, such as the irregular shape of aggregates and the heterogeneous zone around the aggregates [9]. In this study, the aggregates with polished surfaces were embedded in the mortar to minimize the interference caused by the shapes, sizes and relative positions of aggregates in concrete. Thus, the characteristics of ITZ can be evaluated more accurately.

The properties of the ITZ can be affected by the water-cement ratio. To identify the effect of the water-cement ratio on the micro-properties of ITZ, water-cement ratios of 0.30, 0.40, 0.50, and 0.60 were chosen. The designed mix proportions are presented in Table 2. The concrete cubes of 10 mm side length were cast as shown in Fig. 1 (a). Before casting, coarse aggregates of 6 mm ×6 mm × 6 mm were cut and polished and a rubber mold of grid size 10 mm was selected. As shown in Fig. 1 (b), the design thickness of the cement mortar layer of the specimens is 2 mm, which ensures that the cement mortar can be completely carbonated after 5 hours [66]. The treated cubic coarse aggregate was placed in the middle of the mold and only the bottom surface of the aggregate was in contact with the mold. The mixing of cement mortar components was achieved by using a mortar mixer according to the mix proportions of cement mortar in Table 2. The consistometric value was measured by using a mortar consistency tester to ensure the good fluidity, workability and stability of cement mortar. Then a total of 8 concrete specimens were cast and the test surfaces were polished (Fig. 1 b), four of which were prepared for the supercritical carbonation test. The specimens were then demolded and placed into a curing room for 28 days. The temperature and relative humidity of the curing room were set as 20℃ and 95%, respectively. Both the carbonated and noncarbonated specimens were prepared then for the nanoindentation test, scanning electron microscope (SEM) observations, and the mercury intrusion porosimetry (MIP) test.

**Table 2** Mix proportions of cement mortar.

| Groups | Water-cement ratio | Mix proportions (kg/m$^3$) | | |
|---|---|---|---|---|
| | | Cement | Water | Fine aggregate |
| C03SC | 0.30 | 657 | 203 | 445 |
| C04SC | 0.40 | 510 | 203 | 535 |
| C05SC | 0.50 | 405 | 203 | 618 |
| C06SC | 0.60 | 338 | 203 | 699 |

*Remarks*: C03SC denotes the specimens with the water-cement ratio of 0.3 prepared for the supercritical carbonation test.

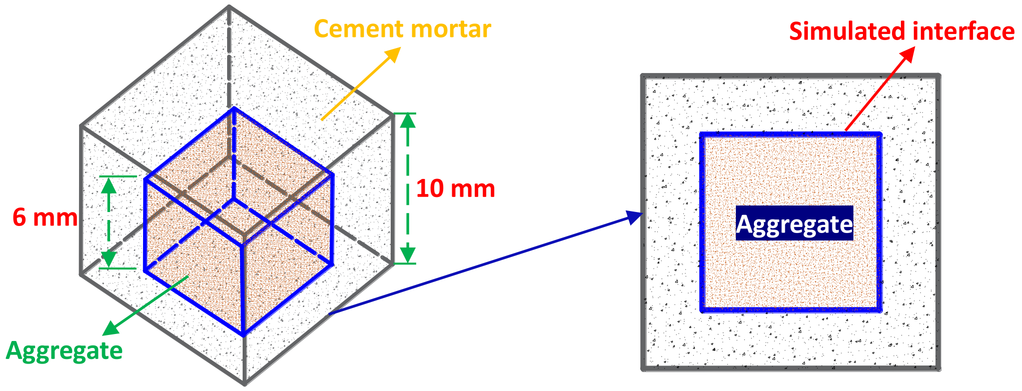


(a) Simulated sample (b) Surface for testing

**Fig. 1.** Simulated interfaces of concrete samples.

*2.3. Procedure of supercritical carbonation*

Fig. 2 shows the supercritical carbonation equipment used to test the prepared concrete specimens. The operation process of supercritical carbonation of concrete with the closed-cycle carbonation system mainly includes four stages: test preparation, increase of $CO_2$ pressure, maintaining of $CO_2$ pressure and recovery of $CO_2$. The concrete specimens were placed in the chamber shown in Fig. 2 (a). The reaction chamber was vacuumed by the vacuum pump and the pressure was measured by the negative pressure gauge shown in Fig. 2 (b). The $CO_2$ was injected into the reaction chamber initially by the pressure difference between the gas cylinders and the reaction chamber until the pressure in the chamber is the same as that of the gas cylinders. Further $CO_2$ injection from the gas cylinder into the reaction chamber was done by the booster pump until the required pressure and temperature in the reaction chamber were reached. The pressure and temperature were adjusted and controlled by the heater and water chiller. After the completion of the supercritical carbonation test, $CO_2$ was driven from the reaction chamber to the gas cylinders by the booster pump and the carbonated concrete specimens were taken out of the chamber. The pressure and temperature in the chamber were continuously recorded during the carbonation process as shown in Fig. 3. The total carbonation time is 6.17 hours, and the supercritical carbonation time is 5 hours, which has completely carbonated the specimens. Some carbonated concrete specimens were cut into two halves. Phenolphthalein solution was applied and sprayed on the cuts to identify whether the concrete specimens were completely carbonated.

The concrete specimens with different water-to-cement ratios before and after supercritical carbonation were prepared for the Nanoindentation, SEM, and MIP tests.

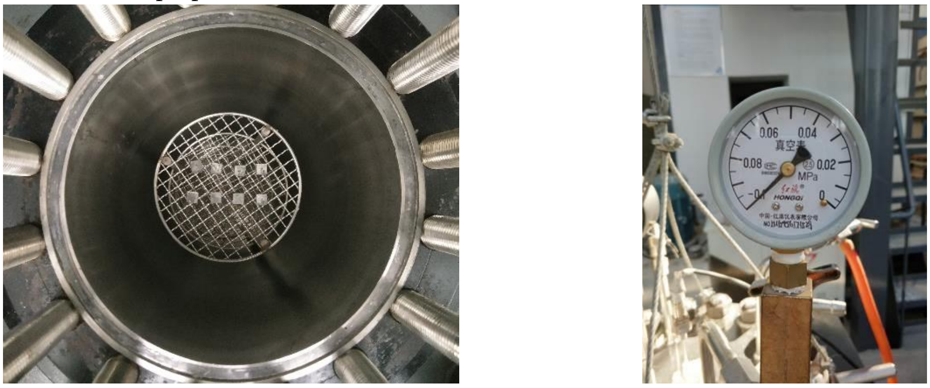

(a) Specimens in the reaction still (b) Negative pressure gauge

**Fig. 2.** Preparation of the supercritical carbonation of concrete.

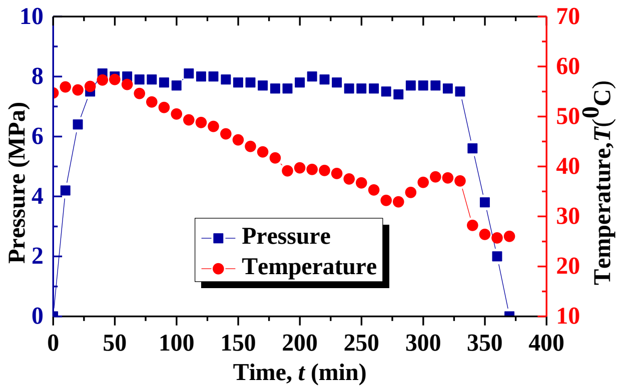


**Fig. 3.** Supercritical carbonation condition.

*2.4. Microscopic test of concrete before and after supercritical carbonation*

*2.4.1. Nanoindentation test*

Nanoindentation was used to characterize the hardness and Young's modulus of ITZ between coarse aggregates and cement paste. The nano-indenter manufactured by the British MML Company was adopted. The indenter was a pyramidal Berkovich diamond indenter. The maximum load of each test point was 2 mN, and the constant loading speed of each test point was 12 mN/min. The load was held for 5s after reaching the maximum load and then unloaded at a constant speed of 12 mN/min. A total of 8 samples were prepared for the Nanoindentation test. Before the supercritical carbonation of concrete specimens, the top surfaces of the specimens were manually ground by using 320, 600 and 1200 grits of abrasive paper and polished using 1 μm alumina for 20 min to achieve smooth surfaces and help identify the microhardness of cement paste, ITZ and aggregates. The preparation of the nanoindentation test of concrete is shown in Fig.

4. As shown in Fig. 4(b), the length of the nanoindentation test zone of each sample is 100 μm and the interval is 10 μm. The cement paste, aggregate and ITZ can be distinguished roughly by the color change. To accurately distinguish the zone of cement paste, aggregate and ITZ, a nanoindentation test was performed continuously and uniformly across the cement paste zone, ITZ and the aggregate zone and the corresponding Vickers hardness values were obtained.

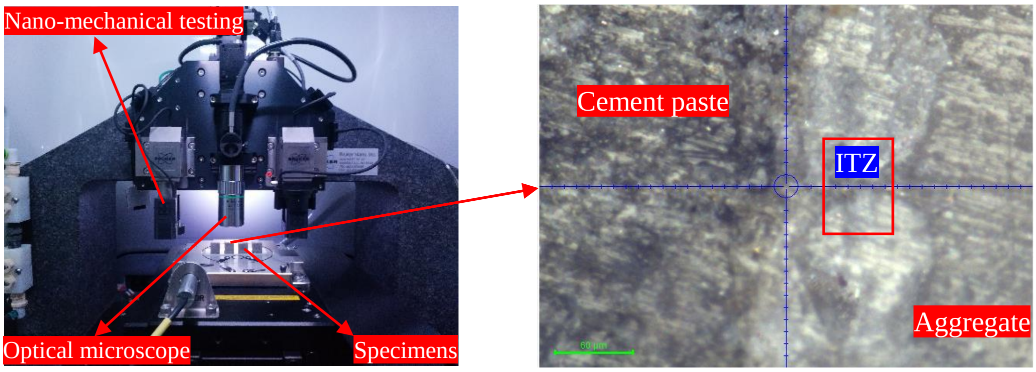


(a) Nano-mechanical testing system (b) Measuring zone

**Fig. 4.** Preparation of nanoindentation test of concrete.

*2.4.2. Scanning electron microscope (SEM) observations*

The microstructure of the interfacial transition zone can be analyzed and characterized by SEM. The phases of concrete, such as pores, unhydrated cement particles, mineral admixture, calcium hydroxide, and hydrated calcium silicate gel, can be distinguished. To study the ITZ, both the noncarbonated and carbonated concrete specimens were broken into small pieces, from which small samples containing both coarse aggregates and cement paste were chosen and polished for further preparation for the scanning electron microscope test. The chosen samples were submerged in absolute alcohol for ultrasonic cleaning to remove dust adsorbed on the fracture surface. The washed samples were then put into a drying vessel with a temperature of 25℃ for 24 hours before they were examined by the SEM with a magnification of 1000. The chemical compositions and relative element contents on the surface of concrete samples before and after supercritical carbonation were finally obtained by energy dispersive spectroscopy (EDS).

*2.4.3. Mercury intrusion porosimetry (MIP) test*

MIP is widely used to obtain pore size distribution of cement-based materials. In order to analyze the changes of porosity of concrete before and after supercritical carbonation, MIP tests were performed by using AutoPore IV 9500 automatic mercury intrusion tester. Before the MIP test, the selected samples were put into absolute ethyl alcohol to stop hydration and then sealed to prevent carbonation. Two carbonated and two noncarbonated samples with the water-cement ratio of 0.4 and 0.5 from those used in the SEM examination were randomly chosen for the MIP test.

## 3. Evolution of ITZ under supercritical $CO_2$ condition

*3.1. Ca/Si ratio and thickness of ITZ*

Quantitative analyses on the element contents from aggregate to cement paste before and after supercritical carbonation were made for Ca and Si by EDS. The Ca/Si ratios distribution around the aggregate of concrete with different water-cement ratios before and after supercritical carbonation are shown in Fig. 5. The red lines and green lines in Fig. 5 represent the change of the element contents of Si and Ca, respectively, and the blue lines represent the change of Ca/Si ratios.

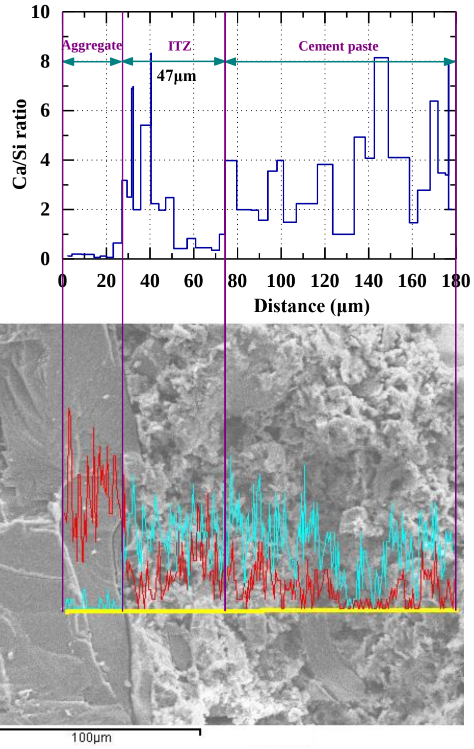


(a) C03SC1, before carbonation

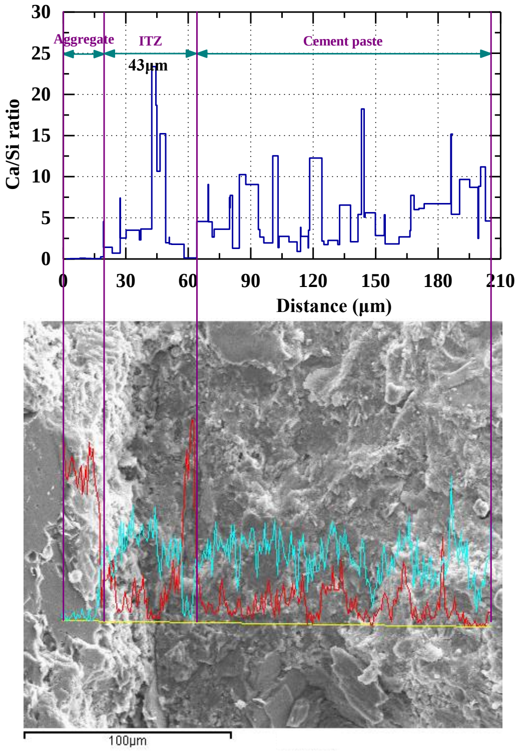


(b) C03SC2, after carbonation

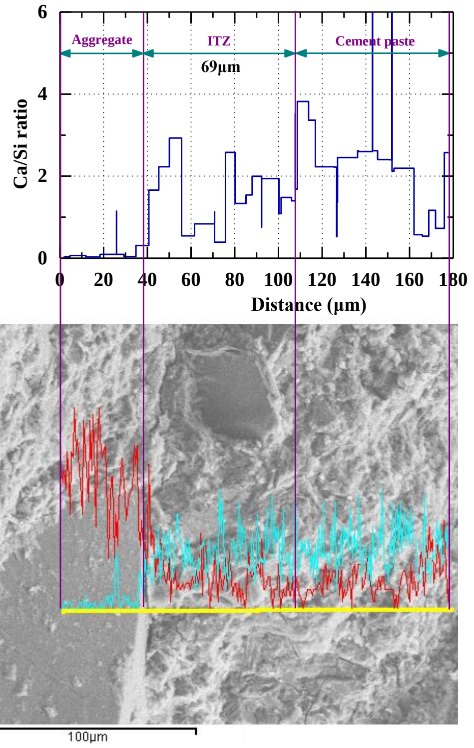


(c) C04SC1, before carbonation

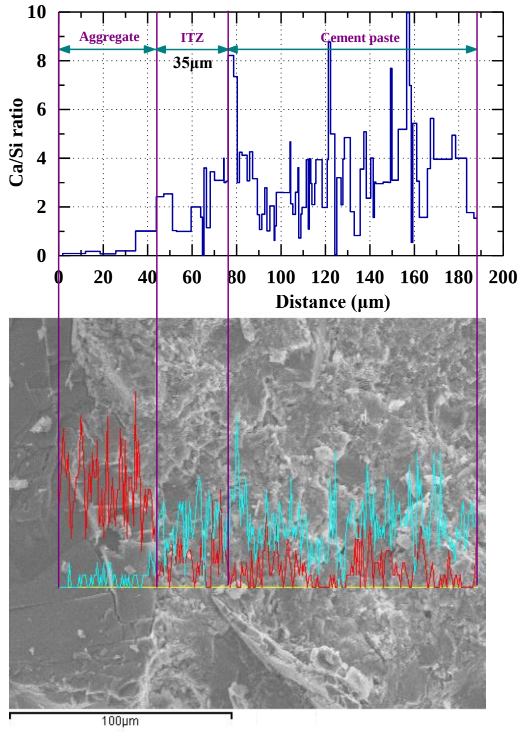


(d) C04SC2, after carbonation

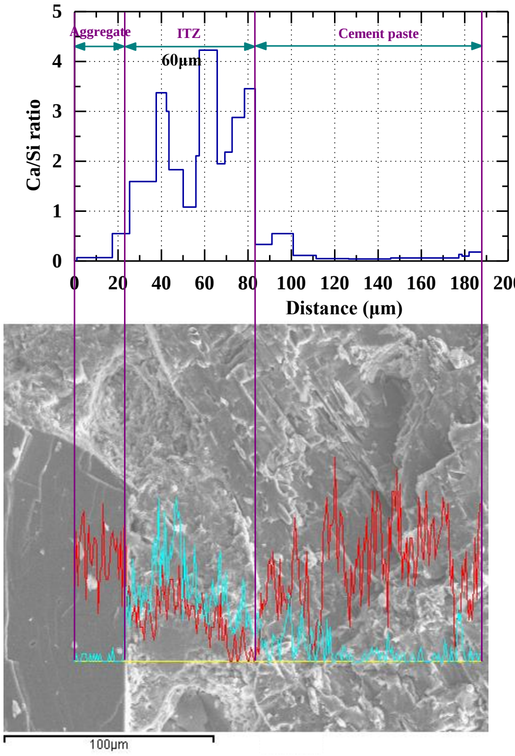


(e) C05SC1, before carbonation

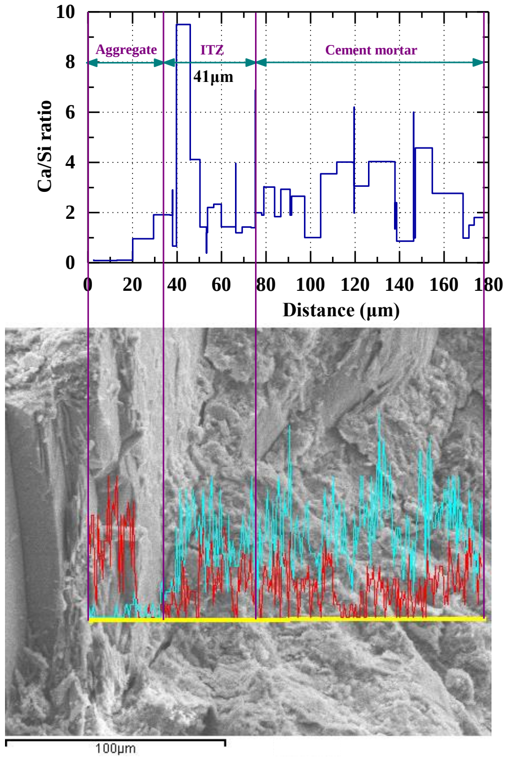


(f) C05SC2, after carbonation

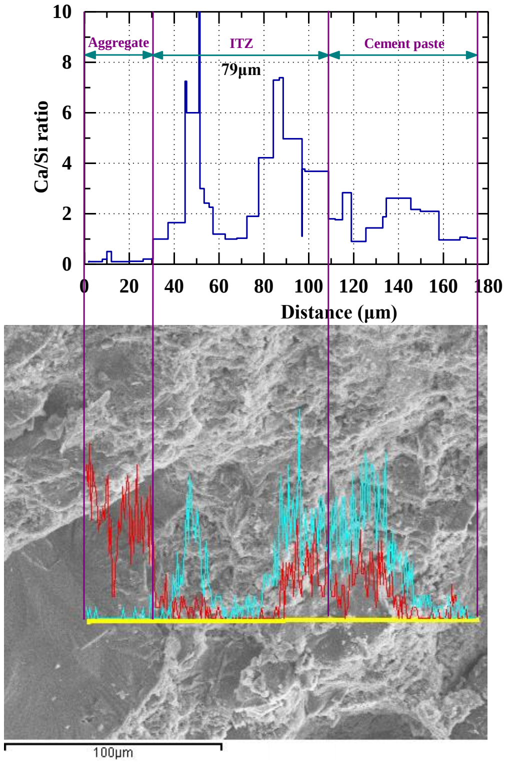


(g) C06SC1, before carbonation

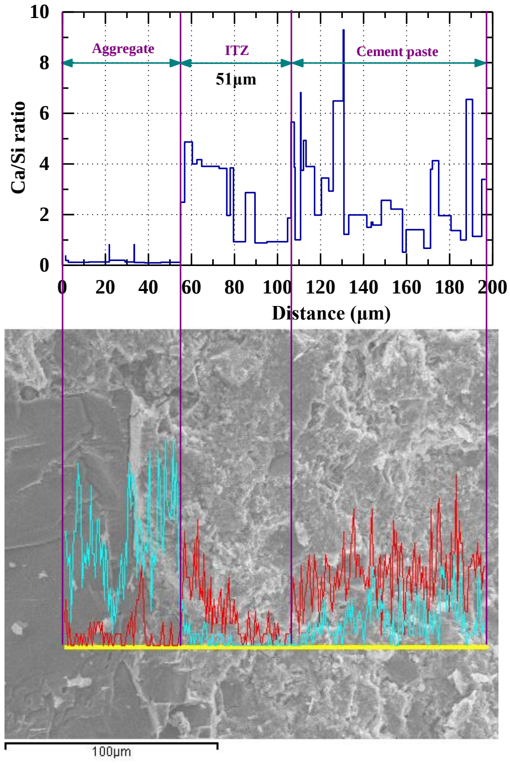


(h) C06SC2, after carbonation

**Fig. 5.** Ca/Si ratios distribution around the aggregate of concrete with different water-cement ratios before and after supercritical carbonation.

As shown in Fig. 5, the aggregate, ITZ and cement paste can be distinguished by the Ca/Si ratios distribution. The ITZ is a thin layer surrounding aggregate, which is characterized by a higher concentration of calcium hydroxide crystals and an increased porosity relative to the cement paste [67,68]. The hydration produces $Ca(OH)_2$ and C-S-H gel with a mean Ca/Si ratio of 1.8-4.9 [69]. Without loss of generality, in the case of the ITZ of the concrete with a water-cement ratio of 0.3 before supercritical carbonation, the Ca/Si ratio dramatically increases from 0.6 to 3.2 around the aggregate boundary at the distance of 27 μm (Fig. 5 a). Then, the Ca/Si ratio gradually decreases to 1.0 at the distance of 74 μm. The average content of Ca in the ITZ is less than that in the cement paste. Thus the thickness of the ITZ is accurately calculated from the difference of the measured distances. For the ITZ of the concrete with the same water-cement ratio after supercritical carbonation (Fig. 5 b), the Ca/Si ratio increases abruptly from 0.3 to 4.5 across the boundary at the distance of 22 μm. The Ca/Si ratios gradually decrease to 1.0 at the distance of 65 μm. Thus the calculated ITZ thickness is 43 μm. By following this process, the calculated ITZ thickness of the concrete sample before and after supercritical carbonation are list in Table 3. The Ca/Si ratios of ITZ and cement paste increase after supercritical carbonation treatment. With the progress of carbonation reaction, $Ca(OH)_2$ continuously dissolves in water and participates in the carbonation reaction, forming $CaCO_3$ and filling pores, which leads to a gradual increase of Ca content in the surface, while the content of Si before and after carbonation has little change. Therefore, the Ca/Si ratio of ITZ and cement paste increases after carbonation.

The ITZ thickness of the concrete with water-cement ratios of 0.3, 0.4, 0.5, and 0.6 varies from 47 μm to 79 μm before supercritical carbonation. The range of the ITZ thickness of the concrete after carbonation is 35-51 μm.

**Table 3** Thickness of ITZ before and after supercritical carbonation.

| Groups | Thickness before carbonation, $t_{ITZ1}$ (μm) | Thickness after carbonation, $t_{ITZ2}$ (μm) | Reduction ratio, $\rho_t$ |
|---|---|---|---|
| C03SC | 47 | 43 | 8.5% |
| C04SC | 69 | 35 | 49.3% |
| C05SC | 60 | 41 | 31.7% |
| C06SC | 79 | 51 | 35.4% |

### *3.2. Microstructure of ITZ*

To study the microstructure of the ITZ, the ITZ between cement paste and aggregates was scanned, by which microscopic morphology of hydration products, such as hydrated calcium silicate gel and ettringite, were clearly shown. Fig. 6 shows the microscopic morphology of the ITZ before and after carbonation at a magnification of 1000×. The left part represents the morphology of the aggregate surface, and the right part is the microtopography of the cement paste at a magnification of 5000×. As shown in Fig. 6, the surface of the coarse aggregates is almost uniform, while the microtopography of the cement paste is uneven with complex hydration products. Cracks can be observed along the surface of the coarse aggregates and cement paste. It demonstrates the incompatibility between the coarse aggregate and the cement paste, and the potential thoroughfare of the supercritical $CO_2$ transport in the concrete. Fig. 6 also clearly shows that the width of micro-cracks between the coarse aggregates and the cement paste is reduced, the overall microstructure is relatively compacted after supercritical carbonation. It can be determined that the structures of calcium hydroxide and C-S-H gel in ITZ are almost undistinguishable from that in cement paste. The porous structure of ITZ may enhance the transport processes of pore liquids, thus allowing frequent moisture changes and continuous dissolution of alkaline substances in ITZ [31].

The ITZ of concrete contained more flaky calcium hydroxides and needle-like amorphous hydrated calcium silicates before supercritical carbonation. A large number of granular calcium carbonates were generated, and the pores were filled after supercritical carbonation, leading to the decrease of porosity and the increase of hardness of ITZ. However, the ITZ is still the weakest zone of concrete despite supercritical carbonation.

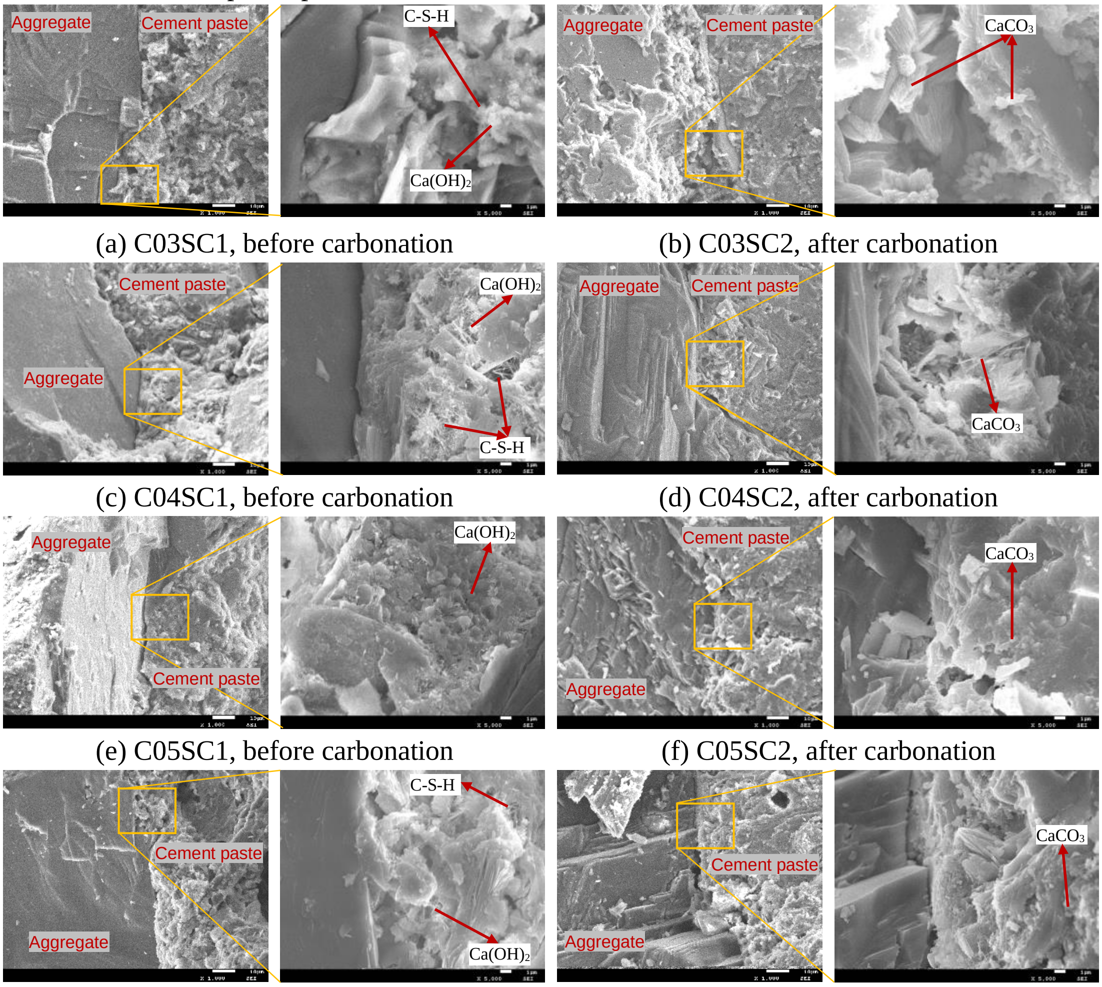


(a) C03SC1, before carbonation (b) C03SC2, after carbonation

(c) C04SC1, before carbonation (d) C04SC2, after carbonation

(e) C05SC1, before carbonation (f) C05SC2, after carbonation

(g) C06SC1, before carbonation (h) C06SC2, after carbonation

**Fig. 6.** SEM images of ITZ of concrete with different water-cement ratios.

*3.3. Microhardness distribution of ITZ*

After the completion of the supercritical carbonation test, the microhardness of the ITZ was examined by a nano-indenter. The tip of the nanoindenter was applied to press into the flat concrete surface according to the loading method mentioned in Section 2. The corresponding loading-unloading curves were obtained, and the modulus and hardness at each measuring point were calculated from the curves. The mechanical properties and microstructure composition of each phase near the ITZ were studied, and the influence of carbonation on the concrete was investigated. The microscopic morphology and microhardness distributions of the ITZ of the concrete with different water-cement ratios are shown in Fig. 7. It can be observed that the cement paste and aggregate can be distinguished by different gray scales. The hardness of the cement paste, the ITZ and the aggregate of the concrete with different water-cement ratios are notably different. The aggregate has the highest hardness, while the ITZ has the lowest. The fluctuation within a component may be attributed to the random distribution of porosity and cracks near the ITZ as well as the existence of defects in the aggregate, as shown in Fig. 4(b). Due to the small amount of hardness distribution data obtained, the aggregate, ITZ and cement paste are roughly distinguished according to the gray level changes of microscopic morphology images and data distribution interval. In order to analyze the hardness distribution of the concrete before and after the supercritical carbonation, the approximate average hardness of the cement paste, the aggregate and the ITZ are calculated and shown in Fig. 7. The horizontal red lines represent the approximate average hardness and the value of cement paste and the ITZ are shown in Table 4.

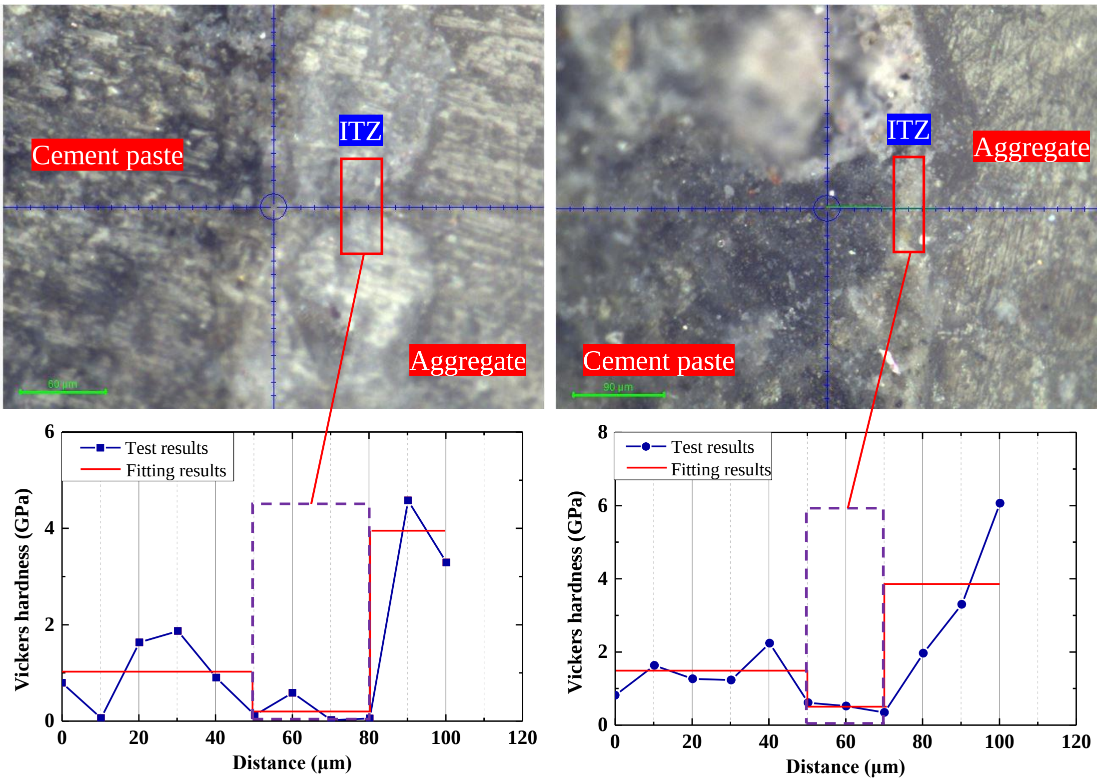


(a) C03SC1, before carbonation (b) C03SC2, after carbonation

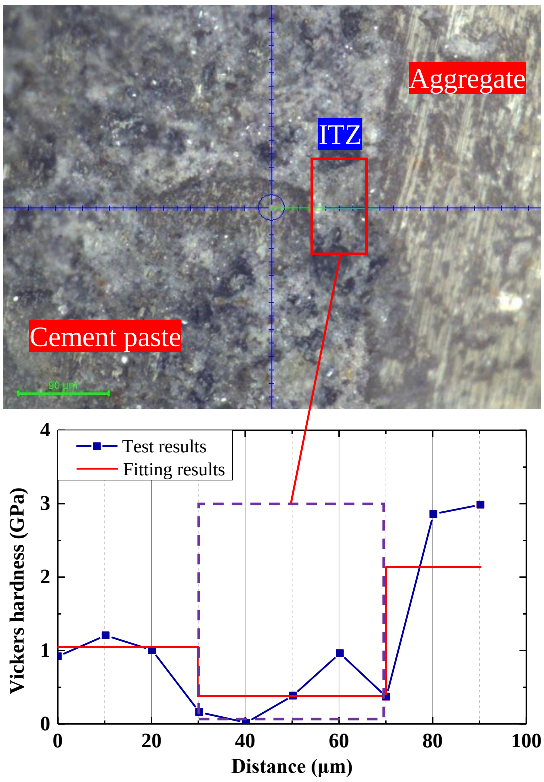


(c) C04SC1, before carbonation

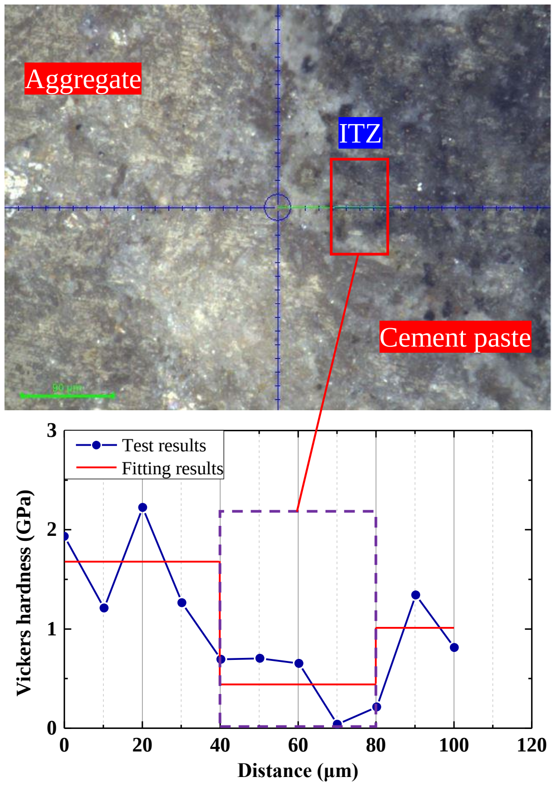


(d) C04SC2, after carbonation

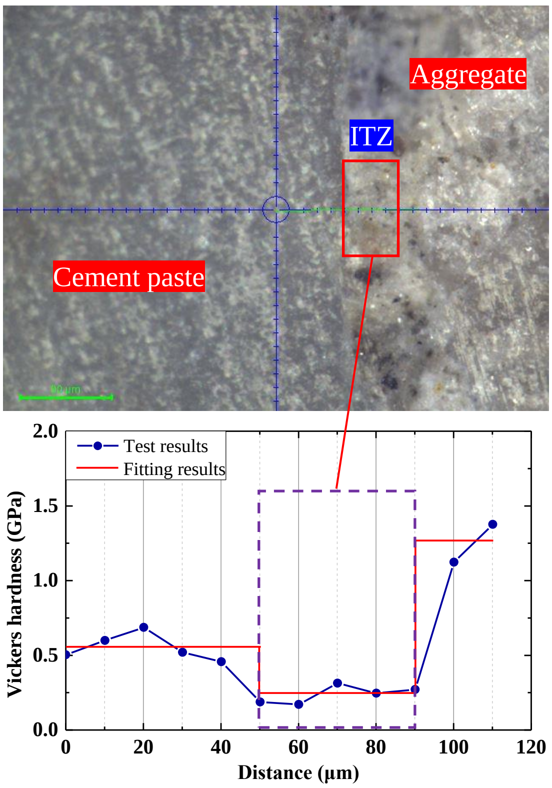


(e) C05SC1, before carbonation

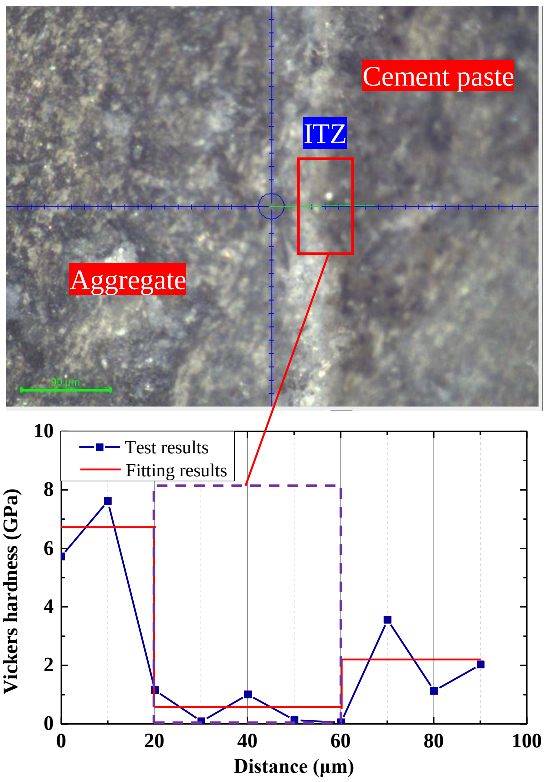


(f) C05SC2, after carbonation

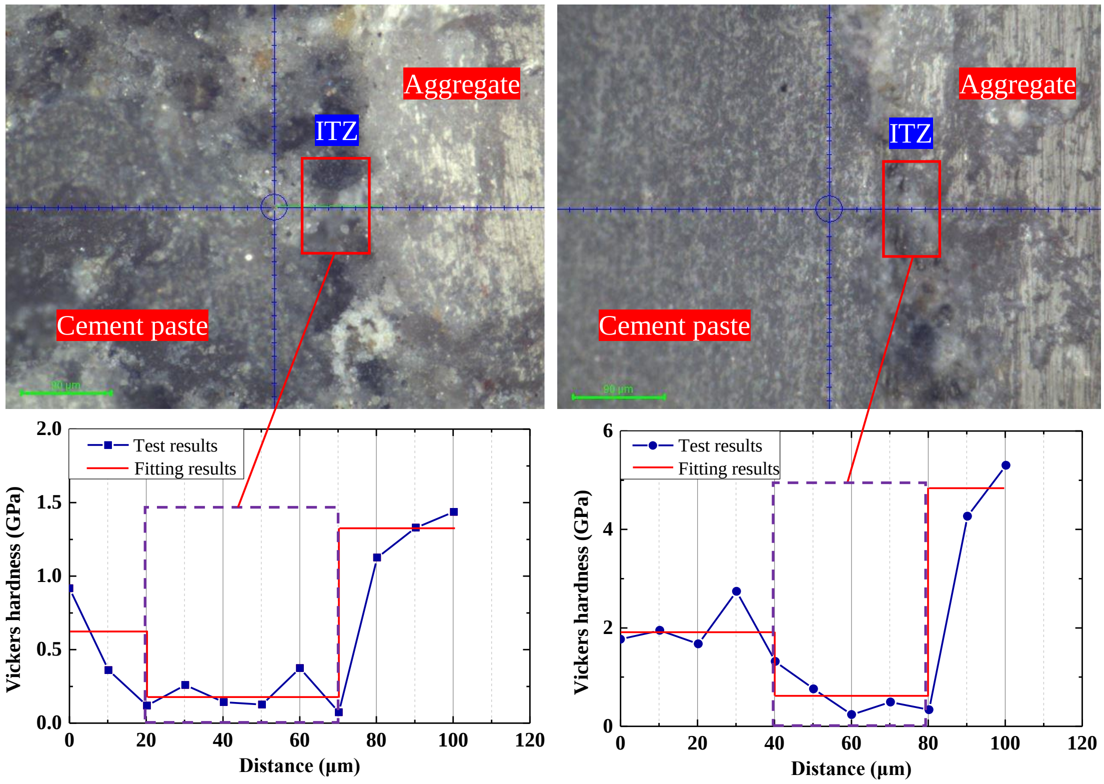


(g) C06SC1, before carbonation (h) C06SC2, after carbonation

**Fig. 7.** Microscopic morphology and hardness distribution of cement paste, ITZ and aggregate of concrete with different water-cement ratios.

**Table 4** Hardness of cement paste and ITZ before and after supercritical carbonation.

| Groups | Average hardness of paste, $h_p$ (GPa) | Average hardness of ITZ, $h_{ITZ}$ (GPa) | $h_p/h_{ITZ}$ |
|---|---|---|---|
| C03SC1 | 1.05 | 0.20 | 5.25 |
| C03SC2 | 1.52 | 0.49 | 3.10 |
| C04SC1 | 1.04 | 0.37 | 2.81 |
| C04SC2 | 1.08 | 0.46 | 2.35 |
| C05SC1 | 0.55 | 0.24 | 2.29 |
| C05SC2 | 2.24 | 0.48 | 4.67 |
| C06SC1 | 0.64 | 0.17 | 3.76 |
| C06SC2 | 1.89 | 0.63 | 3.00 |

As shown in Fig. 7 and Table 4, the thickness of the ITZ can be estimated. The thickness of the ITZ ranges from 20 μm to 55 μm. However, when nanoindentation is applied to quantitatively analyze the thickness of ITZ, the measuring interval is usually 10 microns or more, and the hardness value obtained is also a multiple of ten, which cannot be accurate to single digits. The hardness of the ITZ is about 0.15-0.25 GPa before supercritical carbonation and 0.45-0.50 GPa after supercritical carbonation. There is a sentential increase in the hardness of the ITZ after supercritical carbonation. The hardness of the cement paste is 2-6 times that of the ITZ, which shows that ITZ stays as a weak zone in concrete after carbonation, and may be attributed to the relatively higher water-to-cement ratio and random distribution of defects in ITZ. Although the wide application of nanoindentation in the research of cement-based materials, the hardness measured by the nanoindentation test can be affected by the inhomogeneous distribution of pores and microcracks around ITZ.

### *3.4. Evaluation of porosity of ITZ*

In order to evaluate the porosity of the ITZ before and after supercritical carbonation, MIP tests on the cement paste taken from the concrete with water-cement ratios of 0.4 and 0.5 were carried out before and after supercritical carbonation. The distribution curves of the cumulative intrusion volume of mercury with the pore diameter of cement paste samples were obtained, as shown in Fig. 8. The initial porosities of the cement paste with the water-cement ratio of 0.4 and 0.5 before and after supercritical carbonation are shown in Table 5. The cement paste with a larger water-cement ratio has a larger porosity [70]. The porosity of cement paste was reduced and the material became denser, which is mainly due to the increase of calcium carbonates in the pores of the cement paste after supercritical carbonation [71].

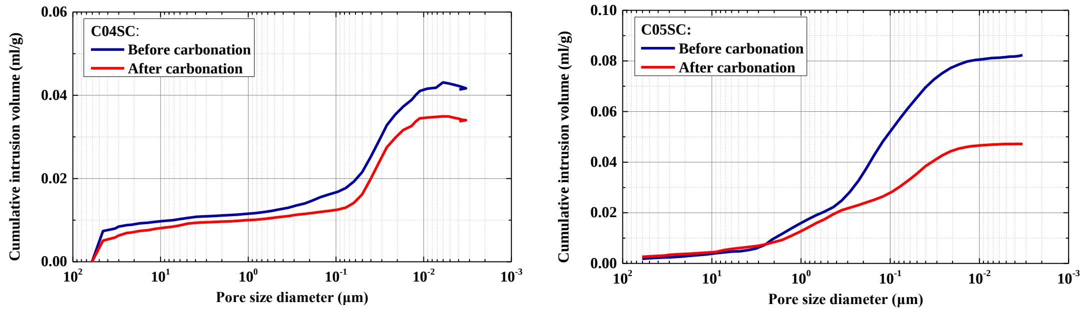


(a) *w/b*=0.40 (b) *w/b*=0.50

**Fig. 8.** Cumulative mercury intrusion vs. pore size diameter curves.

**Table 5** Porosity of cement paste before and after supercritical carbonation.

| Groups | Porosity before carbonation, $n_1$ | Porosity after carbonation, $n_2$ | Reduction ratio, $\rho_n$ |
|---|---|---|---|
| C04SC | 10.86% | 9.32% | 14.2% |
| C05SC | 13.30% | 9.00% | 32.3% |

The nanoindentation techniques have been applied to statistically characterize the nano-mechanical properties of concrete [72,73] and the elasticity and hardness of cement-based materials [40,74]. There is a linear relationship between the porosity and hardness of cement paste [75]. To predict the porosity of ITZ, the effects of porosity on the mechanical properties of cement paste were firstly studied by comparing hardness and porosity in this study. Then the relationship between hardness and porosity of cement paste was established. It was assumed that the relationship between porosity and hardness of cement paste and ITZ is similar. Finally, the porosity of ITZ can be evaluated and calculated according to the value of the hardness of ITZ.

In this section, the measured hardness of cement paste and the ITZ are compared with the porosity of the cement paste with water-cement ratios of 0.4 and 0.5 before and after the supercritical carbonation. The relationship between the hardness and porosity of the cement paste is proposed from the experimental results presented in Table 4 and Table 5. The linear relations between the hardness and porosity of ITZ with the water-cement ratio of 0.4 and 0.5 can be derived from the solution of a binary linear equation and shown in Eq. (1).

$$h_{ITZ} = \begin{cases} -2.6n_{ITZ} + 1.32 & w/c = 0.4 \\ -39.3n_{ITZ} + 5.78 & w/c = 0.5 \end{cases} \tag{1}$$

where $h_{ITZ}$ and $n_{ITZ}$ denote the hardness and porosity of ITZ, respectively.

By the above formula, the porosity of the ITZ of the concrete with a water-cement ratio of 0.4 before and after supercritical carbonation are 36.5% and 33.0%, respectively. These are reduced, respectively, to 14.1% and 13.5%, when the water-cement ratio is 0.5.

## 4. Effect of ITZ on the carbonation depth of concrete under supercritical $CO_2$ condition

### *4.1. Establishment of the geometrical and physical model of concrete*

#### *4.1.1. Random porosity model of concrete*

In consideration of the spatial and inhomogeneous distribution of porosity, it is assumed that the porosity obeys the lognormal distribution. The control equation of the spatial correlation function shown in Eq. (2) is considered to describe the random distribution of porosity of concrete.

$$\phi(x, y) = \exp\left[-\left(\frac{x^2}{a^2} + \frac{y^2}{b^2}\right)^{\frac{1}{1+r}}\right] \tag{2}$$

where $a$ and $b$ denote the autocorrelation lengths, respectively. $r$ is the roughness factor that is 0 in this paper. The Fourier transform and inverse Fourier transform of Eq. (2) are used to generate the random porosity model of concrete. More details of the generation process of the random porosity model can be found in Yu [76]. The value of $a$ and $b$ are assumed as 0.01 m [66]. The average porosity of concrete before supercritical carbonation is 0.133 and the coefficient of variation of porosity is selected as 0.4 [66]. It is assumed that the porosity of the coarse aggregates is 0 for the impermeable property of aggregates [77]. The random distribution of porosity from the above calculations is shown in Fig. 9 (a).

#### *4.1.2. Random aggregate model of concrete*

First, the Monte Carlo method is applied to generate random circular aggregates. Then, the coordinates of the center and the areas of each of the circular aggregates are obtained. The centers of each of the circular aggregates are taken as the control points to generate the polygonal Voronoi diagram. The vertexes of each polygonal Voronoi cell are taken as the control point and the closed B-spline curves are generated by connecting the vertexes to characterize the shape of pebble aggregates. Next, the evenly distributed nodes are selected from the closed B-spline curves to generate convex polygons to characterize the shape of crushed stone aggregates. A proportional area reduction procedure is followed to ensure that the areas of the generated crushed stones are approximately equal to the areas of the initially generated circular aggregates at the corresponding locations. Finally, a two-dimensional random aggregates model of concrete satisfying the given gradation and mix proportion is established. The details of the generation process of the random aggregate model can be found in Bao [78]. The distribution of coarse aggregates is shown in Fig. 9 (b).

*4.1.3. Distribution model of ITZ*

The distribution of ITZ is also considered in the geometrical and physical model of concrete along with the random distribution of coarse aggregates. The distribution model of ITZ was proposed based on the random aggregate model of concrete. The generation process of ITZ is described in detail as follows:

(1) Firstly, the vertex coordinates of each convex polygon of the crushed stone aggregate are obtained.

(2) Then the boundaries of each convex polygon are extended in parallel to the original boundary by a distance equal to the thickness of ITZ.

(3) The area created between the extended and the original boundaries of the crushed stone is the ITZ.

The distribution of ITZ around the coarse aggregates with a thickness of 100 μm is shown in Fig. 9 (c).

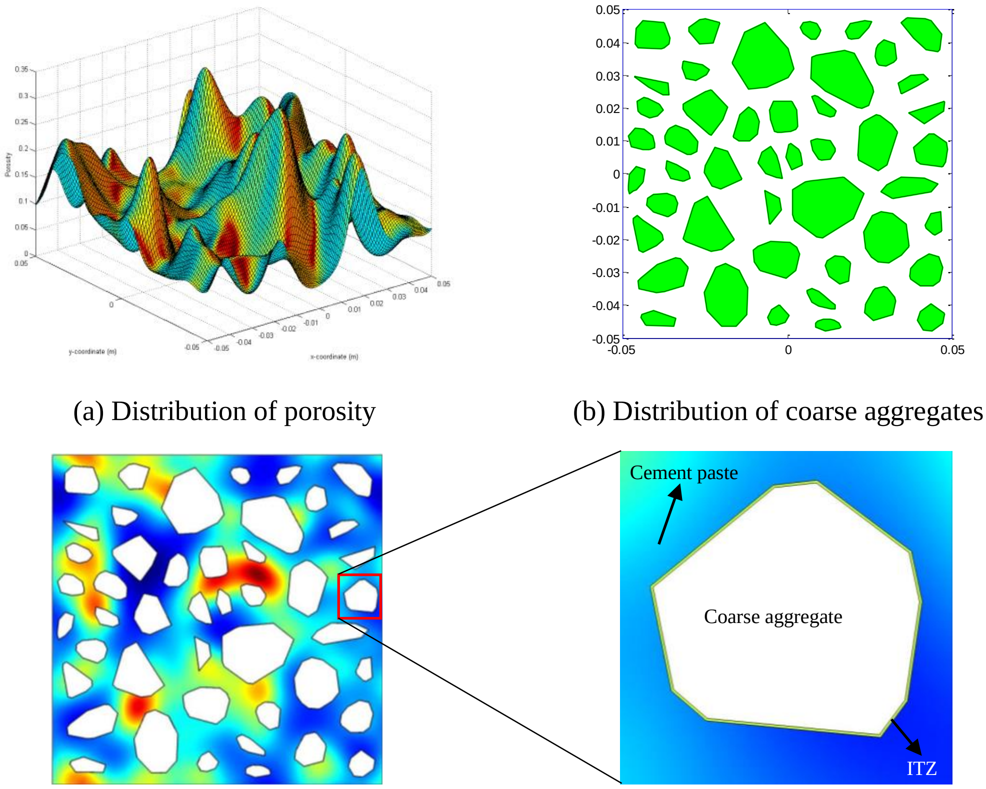


(a) Distribution of porosity

(b) Distribution of coarse aggregates

(c) Distribution of ITZ around the coarse aggregates

**Fig. 9.** Geometrical model considering the distribution of porosity, coarse aggregates and ITZ.

*4.1.4. Supercritical carbonation model of concrete*

In previous studies [49,57,66], the authors have developed a multiphysics supercritical carbonation model that is capable of considering chemical reactions, mass transfer of liquid and gas, dissolution and diffusion of $CO_2$ in water, and energy balance of porous media during the process of supercritical carbonation. The governing equations are shown in Eqs. (3-7).

$$\frac{\partial R_c}{\partial t} = \alpha_1 \times f_1(h) \times f_2(g_v) \times f_3(R_c) \times f_4(T) \tag{3}$$

$$\frac{\partial (g)}{\partial t} = \frac{\partial (m_{co_2})}{\partial t} \tag{4}$$

$$\frac{\partial (nS_\alpha \rho_\alpha)}{\partial t} + \nabla \cdot (\rho_\alpha \vec{u}_\alpha) = q_\alpha \tag{5}$$

$$\vec{u}_\alpha = -\frac{kk_{r\alpha}}{\mu_\alpha}(\nabla P_\alpha - \rho_\alpha \vec{g}) \tag{6}$$

$$\left(\rho C_q\right)_{eff} \frac{\partial T}{\partial t} = \nabla \cdot \left(k_{eff} \nabla T\right) - \left(C_g \rho_g \vec{u}_g + C_w \rho_w \vec{u}_w\right) \nabla T \tag{7}$$

$$k = k_0 \left(\frac{n}{n_1}\right)^3 \cdot \left(\frac{1-n_1}{1-n}\right)^2 \tag{8}$$

where $R_c$ is the degree of carbonation; $g$ is the mass concentration of $CO_2$ in water; $P_\alpha$ is the pressure of phase $\alpha$; subscript $\alpha$ refers to $w$ for the liquid phase and $g$ for gaseous phase; $T$ denotes temperature; $n$ is the porosity of cement paste. The detailed description of the other parameters can be found in Zha and Yu [49].

The initial and boundary conditions were applied to solve the governing equations. In this study, the conditions are introduced and shown in Eqs. (9-11).

$$R_c = R_{c0} = 0,\ P_g = P_{g0},\ P_w = P_{w0},\ g = g_0 = 0,\ T = T_0,\ t = 0 \ on\ \Omega \tag{9}$$

$$\vec{n} \cdot \nabla R_c = 0,\ \vec{n} \cdot \nabla g = 0 \ on\ \Gamma_2 \tag{10}$$

$$P_g = P_{g,sur},\ P_w = P_{w,sur},\ T = T_{sur} \ on\ \Gamma_1 \tag{11}$$

where $R_{c0}$ is the initial conditions specifying the degree of carbonation; $P_{g0}$ and $P_{w0}$ are the initial water pressure and initial gas pressure, respectively; $g_0$ is the initial concentration of dissolved $CO_2$ in water; $T_0$ is the initial temperature; $\vec{n}$ is the normal vector of the boundary; $\Gamma_2$ and $\Gamma_1$ are the boundary using Neumann's conditions and Dirichlet's conditions, respectively; $P_{g,sur}$ and $P_{w,sur}$ are the surrounding gas and liquid pressure, respectively; $T_{sur}$ is the surrounding temperature. The detailed information about the other parameters can be found in Zha [49] and Yu [76].

*4.1.5. Geometrical and physical model of concrete*

In the present study, the geometrical and physical model is developed to include the random distribution model of aggregates, porosity, ITZ and the supercritical carbonation model of concrete. The numerical simulation method of supercritical carbonation of concrete is summarized in Fig. 10. In the simulation, the random distribution of porosity of cement paste was generated by the autocorrelation length and coefficient of variation of porosity, derived from previous research [66,78]. The distribution of ITZ of concrete was generated by considering the porosity and the thickness of ITZ. The coarse aggregates were randomly generated as discussed in Section 4.1.2.

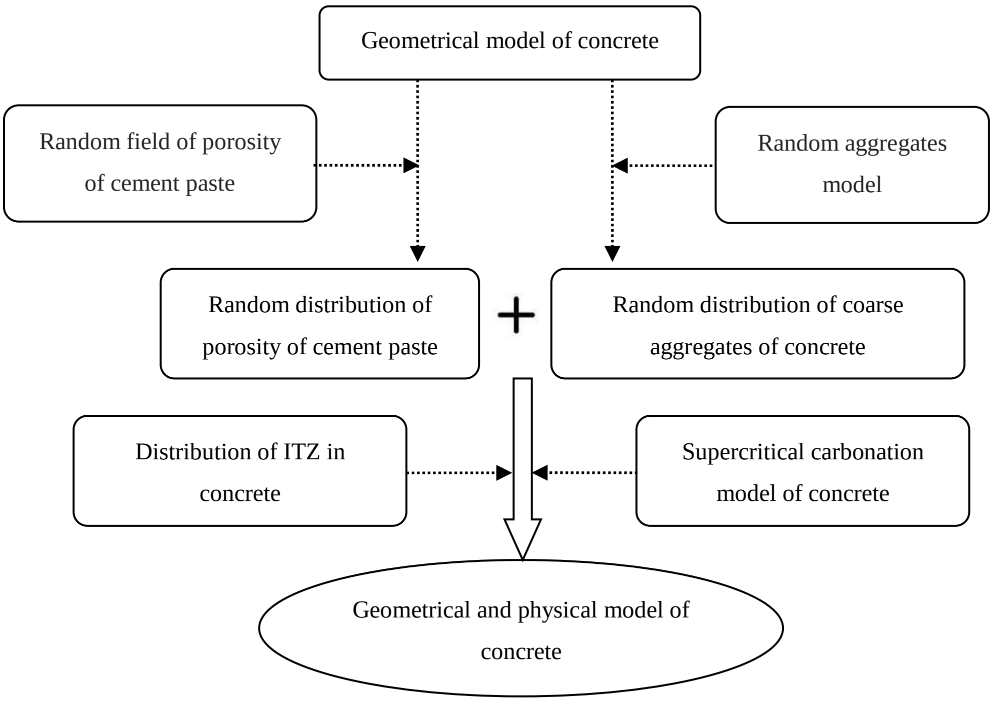


**Fig. 10.** Schematic diagram of a microscopic numerical simulation of supercritical carbonation of concrete.

The thickness and porosity of ITZ are the two main factors affecting the performance of concrete. The carbonation depth is interfered with by many factors, such as concrete aggregates, porosity, etc., and the influence of the ITZ on the supercritical carbonation depth of concrete cannot be stripped out by experiments. In addition, as the thickness of the ITZ is only tens of microns, it is difficult to cast specimens with different ITZ thicknesses. In this section, the effect of ITZ on the carbonation depth of concrete under supercritical $CO_2$ condition is numerically investigated because of the difficulties in experimental testing. The supercritical carbonation of concrete with a water-cement ratio of 0.5 has been verified against experiments in our previous study [78]. Without loss of generality, the effects of ITZ on the carbonation depth of concrete with a water-cement ratio of 0.5 under supercritical $CO_2$ condition were numerically investigated based on the verified model. To eliminate the influence of the random distribution of porosity on carbonation depth, it is assumed that the porosity of cement paste before supercritical carbonation is uniformly distributed, and is 0.133 as shown in Table 5.

*4.2. Effect of the thickness of ITZ*

To study the effect of the thickness of ITZ on the carbonation depth of concrete, the thickness of ITZ was assumed to be 0 μm, 20 μm, 40 μm, 60 μm, 80 μm, and 100 μm, respectively. The porosity of ITZ was assumed to be 19.95%, which is 1.5 times higher than the porosity of cement paste. The supercritical carbonation time was set as 5 hours. The carbonation profiles and the zoomed-in local details are shown in Fig. 11. It can be seen from the magnified local images that the thickness of the ITZ has a certain influence on the distribution of carbonation depth. To further quantitatively analyze the effect of the thickness of ITZ on the carbonation depth, the average value and variance of carbonation depth of concrete with different thicknesses of ITZ are calculated [66] and shown in Table 6. When the thickness of ITZ is 0, only the effect of coarse aggregate on the carbonation depth of concrete was considered. The average and variance of carbonation depth increase with the increase of the thickness of ITZ. As the results of the variance of carbonation depth are shown in Table 6, the effect of coarse aggregates on the distribution of carbonation depth of concrete is more obvious than that of ITZ thickness.

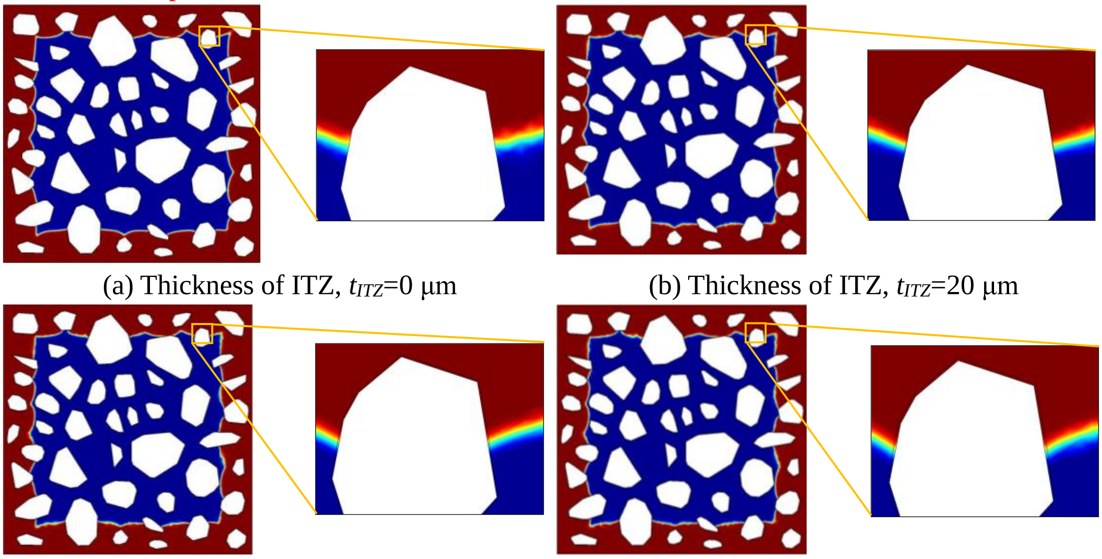

(a) Thickness of ITZ, $t_{ITZ}$=0 μm
(b) Thickness of ITZ, $t_{ITZ}$=20 μm
(c) Thickness of ITZ, $t_{ITZ}$=60 μm
(d) Thickness of ITZ, $t_{ITZ}$=100 μm

**Fig. 11.** Effect of the thickness of ITZ on the supercritical carbonation depth of concrete.

**Table 6** Average value and variance of carbonation depth of concrete with different thicknesses of ITZ.

| Thickness of ITZ, $t_{ITZ}$ (μm) | 0 | 20 | 40 | 60 | 80 | 100 |
|---|---|---|---|---|---|---|
| Average carbonation depth, $D_{ave}$ (mm) | 11.36 | 11.83 | 11.83 | 11.92 | 12.14 | 12.17 |
| Variance of carbonation depth, $V$ (mm$^2$) | 0.60 | 0.63 | 0.68 | 0.72 | 0.74 | 0.74 |

*4.3. Effect of the porosity of ITZ*

In order to study the effect of the porosity of ITZ on the carbonation depth, the porosity of ITZ was assumed to be 13.3%, 19.95%, 26.6%, and 32.25%, respectively, which is 1.0, 1.5, 2.0, and 2.5 times of the porosity of the cement paste. The thickness of ITZ was assumed to be 100 μm. The supercritical carbonation time was also set as 5 hours. The simulation results of carbonation profiles and the zoomed-in details are shown in Fig. 12. As can be seen, the carbonation depth can be significantly affected by the porosity of ITZ according to the zoomed-in images of the simulation results. To quantitatively study the influence of porosity of ITZ on the distribution of carbonation depth, the average and the variance of carbonation depth of the concrete with different porosity of ITZ are calculated and shown in Table 7. When the porosity of ITZ is the same as that of the cement paste, only the effect of coarse aggregate on the carbonation depth of concrete is analyzed. Table 7 shows that the average value and variance of carbonation depth increase with the increase of the porosity of the ITZ. As the results of the variance of carbonation depth are shown in Table 7, when the porosity of ITZ is 33.25%, the average and variance of carbonation depth are increased by 22.2% and 283.3% respectively compared with the porosity of ITZ is 13.3%. The influence of the porosity of ITZ on the distribution of carbonation depth is more obvious than that of the coarse aggregates of concrete. The effect of ITZ porosity on carbonation depth cannot be ignored.

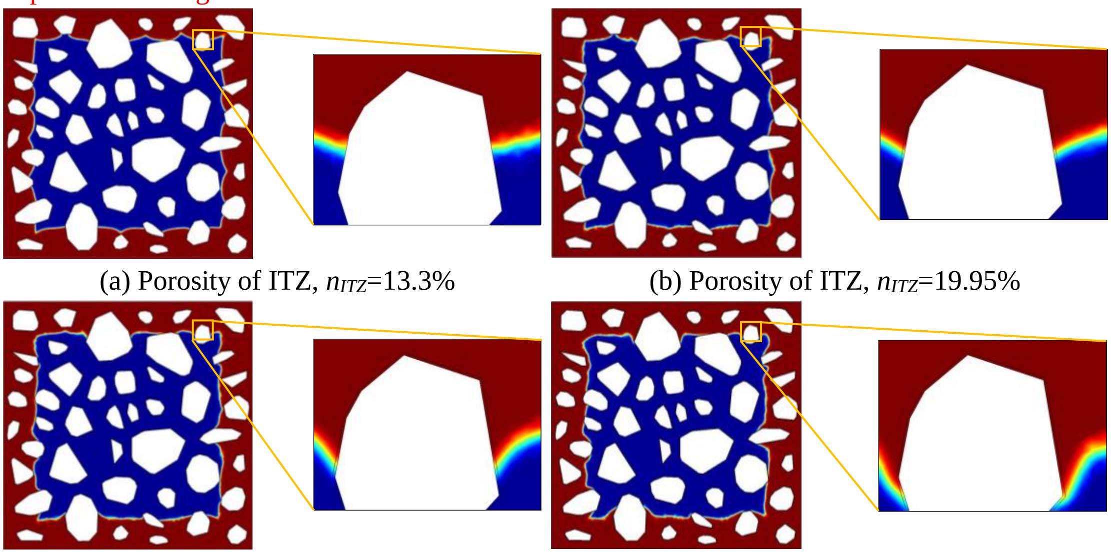

(a) Porosity of ITZ, $n_{ITZ}$=13.3% (b) Porosity of ITZ, $n_{ITZ}$=19.95%

(c) Porosity of ITZ, $n_{ITZ}$=26.6% (d) Porosity of ITZ, $n_{ITZ}$=33.25%

**Fig. 12.** Effect of the porosity of ITZ on the supercritical carbonation depth of concrete.

**Table 7** Average value and variance carbonation depth of concrete with different porosity of ITZ.

| Porosity of ITZ, $n_{ITZ}$ | 13.3% | 19.95% | 26.6% | 33.25% |
|---|---|---|---|---|
| Average carbonation depth, $D_{ave}$ (mm) | 11.36 | 12.17 | 12.71 | 13.88 |
| Variance of carbonation depth, $V$ (mm$^2$) | 0.60 | 0.74 | 0.94 | 2.30 |

## 5. Conclusion

In this paper, nanoindentation, SEM and MIP tests were carried out on concrete specimens of different water-to-cement ratios before and after the supercritical carbonation. The evolution of the ITZ of concrete under supercritical $CO_2$ condition was studied by analyzing the microhardness distribution and microstructure of the ITZ. The thickness of the ITZ was determined by the distribution of Ca/Si ratio across the interface of the coarse aggregates and cement paste. The porosity of the ITZ was also evaluated. The effect of the thickness and porosity of the ITZ on the carbonation depth of concrete under supercritical $CO_2$ condition was numerically investigated using an experimentally validated multiphysics model. The following conclusions can be drawn from the study.

(1) Cracks, pores, calcium carbonates, and C-S-H gel can be observed at the interface of coarse aggregates and cement paste from the SEM characterization results. The microstructures are relatively compacted after supercritical carbonation.

(2) The thickness of ITZ of concrete can be determined by the distribution of Ca/Si ratio across the interface of coarse aggregates and cement paste. The thickness of ITZ of concrete with different water-cement ratios varies from 47 μm to 79 μm before supercritical carbonation and ranges between 35 μm and 51 μm after supercritical carbonation.

(3) The porosity of an ITZ can be estimated by the proposed relational model between the hardness and porosity of cement paste and ITZ.

(4) The distribution of porosity, coarse aggregates, ITZ, and the supercritical carbonation of concrete can be simultaneously considered in the geometrical and physical model.

(5) The average value and variance of carbonation depth of concrete increase with the increase of the thickness and porosity of ITZ. Compared with the thickness of ITZ, carbonation depth of concrete is more sensitive to porosity than thickness of ITZ.

## Credit Author Statement

**Hao Bao:** Methodology, Investigation, Software, Writing-original draft. **Gang Xu:** Conceptualization, Data curation. **Min Yu:** Conceptualization, Software, Visualization, supervision. **Qing Wang:** Software. **Rende Li:** Investigation. **Mohamed Saafi:** Writing-reviewing. **Jianqiao Ye:** Conceptualization, Writing- reviewing and editing, supervision.

## Acknowledgement

The authors are grateful for the Natural Science Foundation of Hubei Province (2020CFB272), the Scientific Research Program of Hubei Provincial Department of Education (Q20201207), the Opening Foundation of Hubei Key Laboratory of Disaster Prevention and Mitigation (Grant No. 2020KJZ01) and the Natural Science Foundation of Yichang (A20-3-012).

## References

[1] A. Leemann, R. Loser, B. Münch, Influence of cement type on ITZ porosity and chloride resistance of self-compacting concrete, Cement and Concrete Composites, 32(2010) 116-120.

[2] R. Liu, H. Xiao, J. Liu, S. Guo, Y. Pei, Improving the microstructure of ITZ and reducing the permeability of concrete with various water/cement ratios using nano-silica, J MATER SCI, 54(2019) 444-456.

[3] N. Otsuki, S. Miyazato, W. Yodsudjai, Influence of Recycled Aggregate on Interfacial Transition Zone, Strength, Chloride Penetration and Carbonation of Concrete, J MATER CIVIL ENG, 15(2003) 443-451.

[4] Y. Wang, X. Jiang, S. Wang, W. Yang, W. Liu, F. Xing, K. Yang, P.A.M. Basheer, Influence of axial loads on $CO_2$ and $Cl^-$ transport in concrete phases: Paste, mortar and ITZ, CONSTR BUILD

MATER, 204(2019) 875-883.

[5] D.N. Quang, M.S.H. Khan, A. Castel, T. Kim, Durability and Microstructure Properties of Low-Carbon Concrete Incorporating Ferronickel Slag Sand and Fly Ash, J MATER CIVIL ENG, 31(2019).

[6] F. Faleschini, K. Brunelli, M.A. Zanini, M. Dabalà, C. Pellegrino, Electric Arc Furnace Slag as Coarse Recycled Aggregate for Concrete Production, Journal of Sustainable Metallurgy, 2(2016) 44-50.

[7] G.C. Lee, H.B. Choi, Study on interfacial transition zone properties of recycled aggregate by micro-hardness test, Construction & building materials, 40(2013) 455-460.

[8] S. Weng, C. Yang, S. Cho, K. Yang, The Study of Chloride Ion Transport Behavior of Mortar under Different Storing Environment Temperatures, J MAR SCI TECH-JAPAN, 20(2012) 290-294.

[9] Z. Luo, W. Li, K. Wang, A. Castel, S.P. Shah, Comparison on the properties of ITZs in fly ash-based geopolymer and Portland cement concretes with equivalent flowability, CEMENT CONCRETE RES, 143(2021) 106392.

[10] Y. Xie, D.J. Corr, F. Jin, H. Zhou, S.P. Shah, Experimental study of the interfacial transition zone (ITZ) of model rock-filled concrete (RFC), CEMENT CONCRETE COMP, 55(2015) 223-231.

[11] K. Wu, H. Shi, L. Xu, G. Ye, G. De Schutter, Microstructural characterization of ITZ in blended cement concretes and its relation to transport properties, CEMENT CONCRETE RES, 79(2016) 243-256.

[12] Y. Li, T. Fu, R. Wang, Y. Li, An assessment of microcracks in the interfacial transition zone of recycled concrete aggregates cured by $CO_2$, CONSTR BUILD MATER, 236(2020) 117543.

[13] J. Shafaghat, A. Allahverdi, Using PC clinker as aggregate-enhancing concrete properties by improving ITZ microstructure, MAG CONCRETE RES, 72(2020) 173-181.

[14] C.S. Poon, Z.H. Shui, L. Lam, Effect of microstructure of ITZ on compressive strength of concrete prepared with recycled aggregates, CONSTR BUILD MATER, 18(2004) 461-468.

[15] J. Han, W. Liu, S. Wang, D. Du, F. Xu, W. Li, G. De Schutter, Effects of crack and ITZ and aggregate on carbonation penetration based on 3D micro X-ray CT microstructure evolution, CONSTR BUILD MATER, 128(2016) 256-271.

[16] R. Mi, G. Pan, Q. Shen, Carbonation modelling for cement-based materials considering influences of aggregate and interfacial transition zone, CONSTR BUILD MATER, 229(2019) 116925.

[17] J. Xiao, W. Li, D.J. Corr, S.P. Shah, Effects of interfacial transition zones on the stress－strain behavior of modeled recycled aggregate concrete, CEMENT CONCRETE RES, 52(2013) 82-99.

[18] Q. Shen, G. Pan, H. Zhan, Effect of Interfacial Transition Zone on the Carbonation of Cement-Based Materials, J MATER CIVIL ENG, 29(2017).

[19] F.U.A. Shaikh, Effect of Cracking on Corrosion of Steel in Concrete, INT J CONCR STRUCT M, 12(2018).

[20] P. Faustino, A. Brás, F. Gonçalves, Â. Nunes, Probabilistic service life of RC structures under carbonation, MAG CONCRETE RES, 69(2017) 280-291.

[21] M. Maleki, I. Rasoolan, A. Khajehdezfuly, A.P. Jivkov, On the effect of ITZ thickness in meso-scale models of concrete, CONSTR BUILD MATER, 258(2020) 119639.

[22] G.S.W.Z. SUN, Numerical calculation and influencing factors of the volume fraction of interfacial transition zone in concrete, Science China. Technological sciences, 55(2012) 1515-1522.

[23] P. Vargas, O. Restrepo-Baena, J.I. Tobón, Microstructural analysis of interfacial transition zone

(ITZ) and its impact on the compressive strength of lightweight concretes, CONSTR BUILD MATER, 137(2017) 381-389.

[24] H. Shi, D. Sun, K. Wu, Development on microstructure and numerical simulation of interfacial transition zone, Journal of the Chinese Ceramic Society, 44(2016) 678-685. (in Chinese)

[25] H. Chen, W. Sun, Q. Zhao, L.J. Sluys, P. Stroeven, Effects of fiber curvature on the microstructure of the interfacial transition zone in fresh concrete, Frontiers of architecture and civil engineering in China, 1(2007) 99-106.

[26] J. Xiao, W. Li, Z. Sun, D.A. Lange, S.P. Shah, Properties of interfacial transition zones in recycled aggregate concrete tested by nanoindentation, CEMENT CONCRETE COMP, 37(2013) 276-292.

[27] X.H. Wang, S. Jacobsen, J.Y. He, Z.L. Zhang, S.F. Lee, H.L. Lein, Application of nanoindentation testing to study of the interfacial transition zone in steel fiber reinforced mortar, CEMENT CONCRETE RES, 39(2009) 701-715.

[28] Y. Gao, G. De Schutter, G. Ye, Z. Tan, K. Wu, The ITZ microstructure, thickness and porosity in blended cementitious composite: Effects of curing age, water to binder ratio and aggregate content, Composites Part B: Engineering, 60(2014) 1-13.

[29] T. Akçaoğlu, M. Tokyay, T. Çelik, Effect of coarse aggregate size and matrix quality on ITZ and failure behavior of concrete under uniaxial compression, CEMENT CONCRETE COMP, 26(2004) 633-638.

[30] J.A. Rossignolo, M.S. Rodrigues, M. Frias, S.F. Santos, H.S. Junior, Improved interfacial transition zone between aggregate-cementitious matrix by addition sugarcane industrial ash, CEMENT CONCRETE COMP, 80(2017) 157-167.

[31] B. Pang, Z. Zhou, X. Cheng, P. Du, H. Xu, ITZ properties of concrete with carbonated steel slag aggregate in salty freeze-thaw environment, CONSTR BUILD MATER, 114(2016) 162-171.

[32] D. Sun, K. Wu, H. Shi, L. Zhang, L. Zhang, Effect of interfacial transition zone on the transport of sulfate ions in concrete, CONSTR BUILD MATER, 192(2018) 28-37.

[33] E.J. Garboczi, D.P. Bentz, Digital simulation of the aggregate－cement paste interfacial zone in concrete, J MATER RES, 6(1991) 196-201.

[34] K. Lyu, W. She, H. Chang, Y. Gu, Effect of fine aggregate size on the overlapping of interfacial transition zone (ITZ) in mortars, CONSTR BUILD MATER, 248(2020) 118559.

[35] H. Ma, Z. Li, A Multi-Aggregate Approach For Modeling the Interfacial Transition Zone in Concrete, ACI MATER J, 111(2014).

[36] K. Wu, L. Xu, G.D. Schutter, H. Shi, G. Ye, Influence of the Interfacial Transition Zone and Interconnection on Chloride Migration of Portland Cement Mortar, J ADV CONCR TECHNOL, 13(2015) 169-177.

[37] D.P. Bentz, E.J. Garboczi, Simulation Studies of the Effects of Mineral Admixtures on the Cement Paste-Aggregate Interface Zone, ACI MATER J, 88(1991) 518-529.

[38] A. Cwirzen, V. Penttala, Aggregate–cement paste transition zone properties affecting the salt－frost damage of high-performance concretes, CEMENT CONCRETE RES, 35(2005) 671-679.

[39] L. Li, J. Xiao, D. Xuan, C.S. Poon, Effect of carbonation of modeled recycled coarse aggregate on the mechanical properties of modeled recycled aggregate concrete, CEMENT CONCRETE COMP, 89(2018) 169-180.

[40] M. Wang, Y. Xie, G. Long, C. Ma, X. Zeng, Microhardness characteristics of high-strength cement paste and interfacial transition zone at different curing regimes, CONSTR BUILD MATER, 221(2019) 151-162.

[41] A. Hussin, C. Poole, Petrography evidence of the interfacial transition zone (ITZ) in the normal strength concrete containing granitic and limestone aggregates, CONSTR BUILD MATER, 25(2011) 2298-2303.

[42] A. Bentur, S. Diamond, S. Mindess, The microstructure of the steel fibre-cement interface, J MATER SCI, 20(1985) 3610-3620.

[43] A. Elsharief, M.D. Cohen, J. Olek, Influence of aggregate size, water cement ratio and age on the microstructure of the interfacial transition zone, CEMENT CONCRETE RES, 33(2003) 1837-1849.

[44] A. Bentur, A. Goldman, M.D. Cohen, S. Mindess, S.P. Shah, The Contribution of the Transition Zone to the Strength of High Quality Silica Fume Concretes, MRS proceedings, 114(1987).

[45] H. Zhan, G. Pan, Y. Wang, Microstructure of interface transition zone in concrete under accelerated carbonation, Journal of Southeast University (Natural Science Edition), 45(2015)569-574. (in Chinese)

[46] W. Huiwen, Y. Liyuan, S. Zhonghe, Modificatin of ITZ structure and properties of regenerated concrete, Journal of Wuhan University of Technology-Mater. Sci. Ed, 21(2006) 128-132.

[47] Q. Shen, G. Pan, H. Zhan, Test method to simulate the influence of the interface on the concrete carbonation process, Journal of Wuhan University of Technology-Mater. Sci. Ed., 31(2016) 594-598.

[48] G. Kim, J. Kim, K.E. Kurtis, L.J. Jacobs, Y. Le Pape, M. Guimaraes, Quantitative evaluation of carbonation in concrete using nonlinear ultrasound, MATER STRUCT, 49(2016) 399-409.

[49] X. Zha, M. Yu, J. Ye, G. Feng, Numerical modeling of supercritical carbonation process in cement-based materials, CEMENT CONCRETE RES, 72(2015) 10-20.

[50] B. Zhan, C. Poon, C. Shi, $CO_2$ curing for improving the properties of concrete blocks containing recycled aggregates, Cement and Concrete Composites, 42(2013) 1-8.

[51] S. Kou, B. Zhan, C. Poon, Use of a $CO_2$ curing step to improve the properties of concrete prepared with recycled aggregates, Cement and Concrete Composites, 45(2014) 22-28.

[52] M. Chabannes, E. Garcia-Diaz, L. Clerc, J. Bénézet, Studying the hardening and mechanical performances of rice husk and hemp-based building materials cured under natural and accelerated carbonation, CONSTR BUILD MATER, 94(2015) 105-115.

[53] J. Xiao, J. Li, C. Zhang, Mechanical properties of recycled aggregate concrete under uniaxial loading, CEMENT CONCRETE RES, 35(2005) 1187-1194.

[54] X. Zha, H. Wang, P. Xie, C. Wang, P. Dangla, J. Ye, Leaching resistance of hazardous waste cement solidification after accelerated carbonation, Cement and Concrete Composites, 72(2016) 125-132.

[55] M. FERNANDEZBERTOS, S. SIMONS, C. HILLS, P. CAREY, A review of accelerated carbonation technology in the treatment of cement-based materials and sequestration of $CO_2$, J HAZARD MATER, 112(2004) 193-205.

[56] X. Zha, J. Ning, M. Saafi, L. Dong, J.M. Dassekpo, J. Ye, Effect of supercritical carbonation on the strength and heavy metal retention of cement-solidified fly ash, CEMENT CONCRETE RES, 120(2019) 36-45.

[57] H. Bao, M. Yu, Y. Liu, J. Ye, Performance evaluation of steel-polypropylene hybrid fiber reinforced concrete under supercritical carbonation, Journal of Building Engineering, 43(2021) 103159.

[58] J.B. Rubin, J.W. Carey, C. Taylor, Enhancement of cemented wasted waste forms by supercritical

$CO_2$ carbonation of standard portland cements, 1997, pp.473-478.

[59] K.A. Snyder, D.N. Winslow, D.P. Bentz, E.J. Garboczi, Effects of Interfacial Zone Percolation on Cement-Based Composite Transport Properties, MRS Proceedings, 245(1991).

[60] D.P. Bentz, Influence of internal curing using lightweight aggregates on interfacial transition zone percolation and chloride ingress in mortars, Cement and Concrete Composites, 31(2009) 285-289.

[61] D.P. Bentz, J.T.G. Hwang, C. Hagwood, E.J. Garboczi, K.A. Snyder, N. Buenfeld, K.L. Scrivener, S. Diamond, F.P. Glasser, S. Mindess, L.R. Roberts, J.P. Skalny, Interfacial Zone Percolation in Concrete: Effects of Interfacial Zone Thickness and Aggregate Shape, MRS proceedings, 370(1994).

[62] H. Bao, G. Xu, Q. Wang, Y. Yang, Y. Su, Investigation on the Distribution Characteristics of Partial Carbonation Zone of Concrete, J MATER CIVIL ENG, 33(2021) 3548.

[63] C. Chang, J. Chen, The experimental investigation of concrete carbonation depth, CEMENT CONCRETE RES, 36(2006) 1760-1767.

[64] C.D. Atiş, Accelerated carbonation and testing of concrete made with fly ash, CONSTR BUILD MATER, 17(2003) 147-152.

[65] M. Brouxel, The alkali-aggregate reaction rim: $Na_2O$, $SiO_2$, $K_2O$ and CaO chemical distribution, CEMENT CONCRETE RES, 23(1993) 309-320.

[66] H. Bao, M. Yu, Y. Liu, J. Ye, Experimental and statistical study on the irregularity of carbonation depth of cement mortar under supercritical condition, CONSTR BUILD MATER, 174(2018) 47-59.

[67] Y. Tian, Z. Tian, N. Jin, X. Jin, W. Yu, A multiphase numerical simulation of chloride ions diffusion in concrete using electron microprobe analysis for characterizing properties of ITZ, CONSTR BUILD MATER, 178(2018) 432-444.

[68] D. Breton, A. Carles-Gibergues, G. Ballivy, J. Grandet, Contribution to the formation mechanism of the transition zone between rock-cement paste, CEMENT CONCRETE RES, 23(1993) 335-346.

[69] J.J. Chen, L. Sorelli, M. Vandamme, F. Ulm, G. Chanvillard, A Coupled Nanoindentation/SEM-EDS Study on Low Water/Cement Ratio Portland Cement Paste: Evidence for C-S-H/$Ca(OH)_2$ Nanocomposites, J AM CERAM SOC, 93(2010) 1484-1493.

[70] Z. Lafhaj, M. Goueygou, A. Djerbi, M. Kaczmarek, Correlation between porosity, permeability and ultrasonic parameters of mortar with variable water/cement ratio and water content, CEMENT CONCRETE RES, 36(2006) 625-633.

[71] B. Wu, G. Ye, Development of porosity of cement paste blended with supplementary cementitious materials after carbonation, CONSTR BUILD MATER, 145(2017) 52-61.

[72] L. Sorelli, G. Constantinides, F. Ulm, F. Toutlemonde, The nano-mechanical signature of Ultra High Performance Concrete by statistical nanoindentation techniques, CEMENT CONCRETE RES, 38(2008) 1447-1456.

[73] G. Constantinides, F. Ulm, K. Van Vliet, On the use of nanoindentation for cementitious materials, MATER STRUCT, 36(2003) 191-196.

[74] G. Constantinides, F. Ulm, The effect of two types of C-S-H on the elasticity of cement-based materials: Results from nanoindentation and micromechanical modeling, CEMENT CONCRETE RES, 34(2004) 67-80.

[75] L. Liu, X. Wang, J. Zhou, H. Chu, D. Shen, H. Chen, S. Qin, Investigation of pore structure and mechanical property of cement paste subjected to the coupled action of freezing/thawing and calcium leaching, CEMENT CONCRETE RES, 109(2018) 133-146.

[76] M. Yu, H. Bao, J. Ye, Y. Chi, The effect of random porosity field on supercritical carbonation of cement-based materials, CONSTR BUILD MATER, 146(2017) 144-155.
[77] L. Li, A pore size distribution-based chloride transport model in concrete, MAG CONCRETE RES, 66(2014) 937-947.
[78] H. Bao, M. Yu, L. Xu, M. Saafi, J. Ye, Experimental study and multi-physics modelling of concrete under supercritical carbonation, CONSTR BUILD MATER, 227(2019) 116680.